A REVIEW OF AERONAUTICAL FATIGUE INVESTIGATIONS IN ISRAEL

(April 2009 – March 2011)

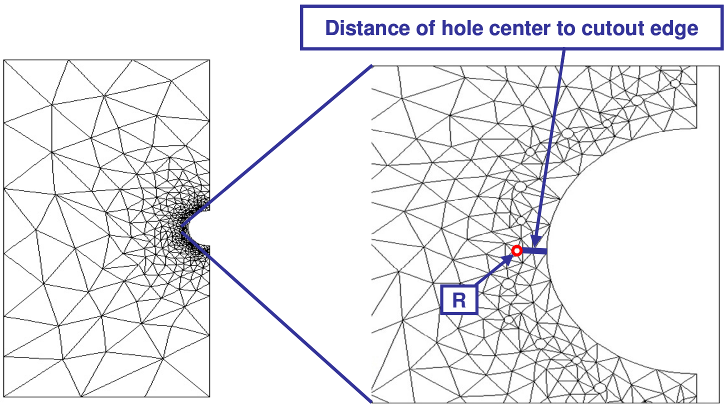

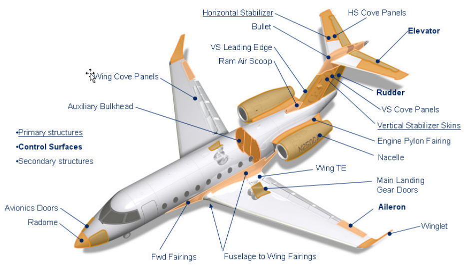

Compiled by:
Abraham Brot
Engineering Division
Israel Aerospace Industries
***Ben-Gurion Airport,* Israel**
abrot@iai.co.il

Presented at the 32nd Conference of the International Committee on Aeronautical Fatigue and Structural Integrity (ICAF)
Montreal, Canada
30 May 2011

Israel Society of Aeronautics and Astronautics האגודה למדעי התעופה והחלל בישראל

IAI ENGINEERING & DEVELOPMENT GROUP
ISRAEL AEROSPACE INDUSTRIES LTD

A REVIEW OF AERONAUTICAL FATIGUE INVESTIGATIONS IN ISRAEL

APRIL 2009 – MARCH 2011

SUMMARY

This review summarizes fatigue, structural-integrity and fracture-mechanics investigations that were performed in Israel during the period April 2009 to March 2011. The review includes contributions from Israel Aerospace Industries Ltd. (IAI), Israel Air Force (IAF), Tel-Aviv University (TAU), and Ben-Gurion University (BGU).

The editor acknowledges the assistance given to him by the Israel Society of Aeronautics and Astronautics in preparing and presenting this document.

Presented at the 32nd ICAF Conference
Montreal, Canada
30 May 2011

TABLE OF CONTENTS

A REVIEW OF AERONAUTICAL FATIGUE INVESTIGATIONS IN ISRAEL APRIL 2009 – MARCH 2011

1 INTRODUCTION

The Israel National Review summarizes work performed in the field of aeronautical fatigue in Israel during the period April 2009 to March 2011. The previous National Review [1] covered aeronautical fatigue activities up to March 2009. The following organizations contributed to this review:

Israel Aerospace Industries Ltd. (IAI)
Israel Air Force (IAF)
Tel-Aviv University (TAU)
Ben-Gurion University (BGU)

The National Review was compiled by Abraham Brot (abrot@iai.co.il).

2 FATIGUE ANALYSIS, TESTING AND LIFE EXTENSION

2.1 Fatigue of an Access Panel Cutout Having Satellite Holes (C. Matias, Y. Matola and A. Brot, IAI)

This activity was first reported upon in the 2009 National Review [1]. During a fatigue test performed on a wing, cracks were discovered at a round access panel cutout having satellite holes, as is shown in Figure 1.

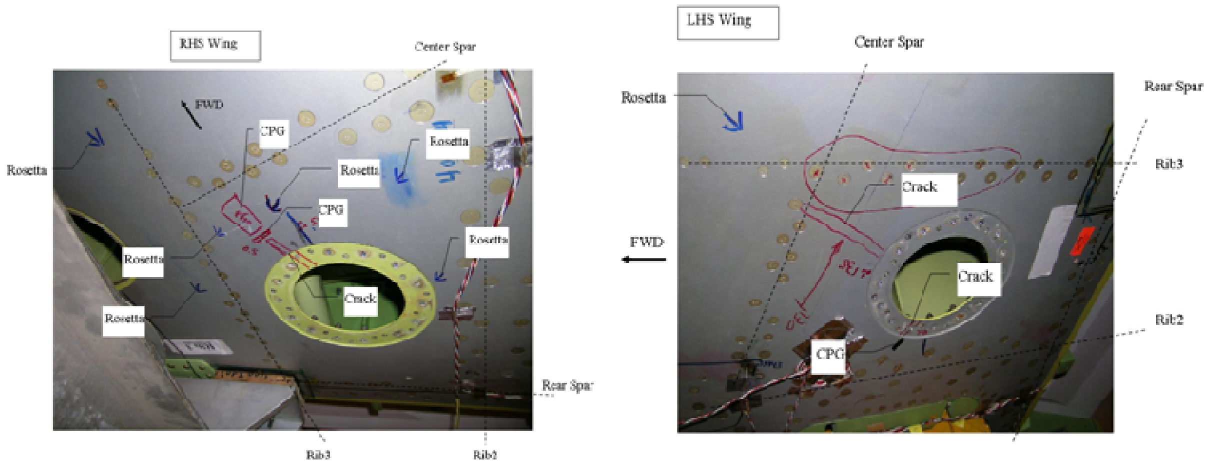

Figure 1: Cracks Discovered at Satellite Holes around an Access Panel Cutout

A component test program was performed at IAI in order to investigate the problem and to evaluate several solutions. Testing was performed on 7457-T7351 aluminum panels having overall dimensions of 900 x 480 mm. The nominal panel thickness is 5.4 mm. The panel cutout has a diameter of 120 mm, with the general configuration shown in Figure 2.

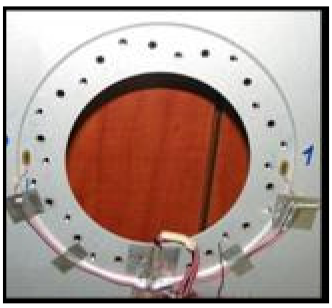

Figure 2: Test Panel Configuration

The satellite holes shown in Figure 2 represent the holes for attaching the access panel cover as well as holes for securing the nut-plates.

The panel was loaded to a typical flight-by-flight randomized wing gust and maneuver spectrum having approximately 18 cycles per flight and having a maximum stress of 19.6 ksi (135 MPa). Strain-gages were installed on both faces of each panel, and crack-propagation gages (CPGs) were used to detect crack-initiation at the satellite holes. Strain-gage readings and NDI were performed periodically.

Two panel configurations were tested: (1) panel with original satellite holes; (2) panel with all satellite holes cold-worked.

Testing showed that both components (without cold-worked fastener holes and with cold-worked fastener holes) failed at very similar lives around 9,000 flights. Clearly, cold-working was not an adequate solution for this problem, and a more complicated solution was implemented.

A 3D nonlinear finite-element model (FEM) was built of the access panel cutout, including the closest fastener hole, using StressCheck Software. (See Figure 3.) For the cold-worked configuration, the cold-working process was simulated by first introducing a 4.1% interference, and then removing it. An external stress of 13.4 ksi was then applied to the FEM. For both cases, the resulting stress at the satellite hole was above the yield-strength of the material, and was very similar for the cold-worked and non-cold-worked configurations. In addition, the countersink at each of the holes and the skin thickness down-step further increased the local stresses. ***It was estimated that $K_t \cong 12$ at the fastener hole, after accounting for all the geometrical details.***

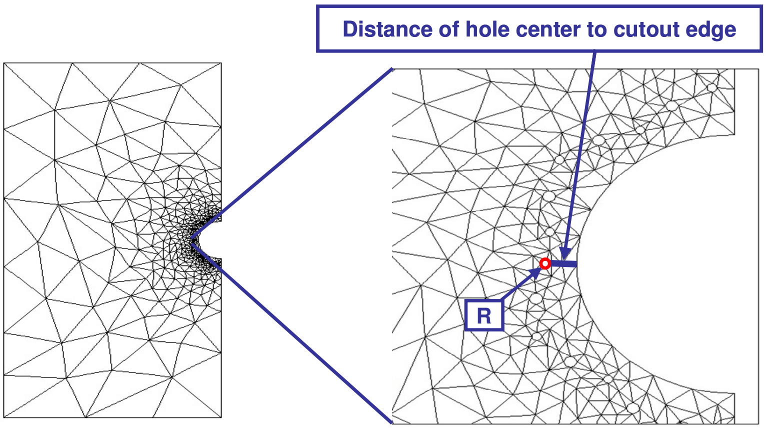

Figure 3: StressCheck FEM Showing the Proximity of the Closest Satellite Hole to the Cutout Edge

From the testing and analysis, it was concluded that the high notch stresses at the satellite hole produced sufficient plasticity so that both the cold-worked and non-cold-worked configurations acted in a similar manner, and the cold-working was not effective in increasing the fatigue life.

Further testing is planned using "ForceTec" inserts (An FTI product) instead of the conventional nutplates, in order to investigate its effect on the fatigue life.

2.2 The Effect of Fastener-Fit and Installation Procedure on Fatigue Life (C. Matias and A. Brot, IAI)

A test program was initiated at IAI to study the effect of fastener interference, as well as the manner of inserting the fastener, on crack-initiation and growth. Each of the specimens will be manufactured from a 7475-T7351 plate having four holes sized to accept a 3/16 inch hi-lok fastener. The specimens will include three levels of fastener interference: clearance-fit, transition-fit (nominal interference of 0.4%) and interference-fit (nominal interference of 1.2%). Fastener insertion will be performed by two methods: by the use of plastic hammers and by the use of pneumatic hammers. The purpose of the investigation is to determine the optimum configuration as well as the optimum manner of inserting the fastener, in order to obtain maximum fatigue life.

2.3 Autofrettaged Thick-Walled Cylinders and Spherical Vessels (M. Perl et al, Ben-Gurion University)

Autofrettage of large diameter tubes (gun barrels) is used to increase the elastic strength of the tube and to increase its fatigue life. It is based on the permanent expansion of the cylinder bore using either hydraulic pressure or an oversize mandrel. The theoretical solution of the autofrettage problem involves different yield criteria, the Bauschinger effect and the recalculation of the residual stress field after machining. Accurate stress-strain data is needed for the numerical analysis of the residual stress field due to autifrettage. Although this topic does not relate directly to aeronautical fatigue, it was included in this review because of the similarity of the autofrettage process to that of the cold-working process that is used extensively in aircraft structures. This research is a direct continuation of previous work presented in the 2009 Israel National Review [1]. Four investigations are summarized here. Three deal with autofrettage of cylindrical or spherical geometries. One deals with a spherical pressure vessel manufactured by the IHBF process.

In order to maximize the performance of modern gun barrels in terms of strength-to-weight ratio and total fatigue life, favorable compressive residual stresses are introduced to the inner portion of the barrel, commonly by the autofrettage process. There are two major autofrettage processes for overstraining the tube: the hydrostatic, and the swage. There are several theoretical solutions for hydrostatic autofrettage, based on Lamé's solution and the von Mises or Tresca yield criteria. The residual stress field due to hydraulic autofrettage is treated as an axisymetric, two-dimensional problem solved in terms of the radial displacement solely. Once the Bauschinger effect was included in these models they yield very realistic results. Unlike in the case of hydraulic autofrettage, swage autofrettage needs to be modeled by a three-dimensional model. The present analysis suggests a new 3-D axisymmetric model for solving the residual stress field due to swage autofrettage in terms of both the radial and the axial displacements. The axisymetric equilibrium equations are approximated by finite differences and solved then by Gauss-Seidel method. Using the new computer code the stresses, the strains, the displacements and the forces are determined [2]. A full-scale instrumented swage autofrettage test was conducted and the numerical results were validated against the experimental findings. The calculated strains, the permanent bore enlargement, and the mandrel pushing force were found to be in very good agreement with the measured values [2].

Many spherical pressure vessels are manufactured by methods such as the Integrated Hydro-Bulge Forming (IHBF) method, where the sphere is composed of a series of double curved petals welded along their meridional lines. (See Figure 4.) Such vessels are susceptible to multiple radial cracking along the welds. For fatigue life assessment and fracture endurance of such vessels one needs to evaluate the Stress Intensity Factors (SIFs) distribution along the fronts of these cracks**.** However, to date, only two 3-D solutions for the SIF for ***one*** inner semi-elliptical crack in thin or thick spheres are available, as well as 2-D SIFs for ***one*** through the thickness crack in thin spherical shells. In the present paper, mode I SIF distributions for a wide range of lunular and crescentic cracks are evaluated. The 3-D analysis is performed, via the FE method employing singular elements along the crack front, for a typical spherical pressure vessel with outer to inner radius ratios of $\eta=R_o/R_i=1.1$. SIFs are evaluated for arrays containing n=1-20 cracks; for a wide range of crack depth to wall thickness ratio, a/t, from 0.025 to 0.95; and for various ellipticities of the crack, i.e., the ratio of crack depth to semi crack length, a/c, from 0.2 to 1.5. The obtained results clearly indicate that the SIFs are considerably affected by the three-dimensionality of the problem, and the following parameters: the number of cracks in the array-n, the relative crack depth -a/t, and the crack ellipticity-a/c [3].

Figure 4: A Liquefied Petroleum Gas (LPG) Spherical Tank Formed by the Integrated Hydro-Bulge Forming (IHBF)Method

Increased strength-to-weight ratio and extended fatigue life are the main objectives in the optimal design of modern pressure vessels. These two goals can mutually be achieved by creating a proper residual stress field in the vessel's wall, by a process known as autofrettage. Although there are many studies that have investigated the autofrettage problem for cylindrical vessels, only few such studies exist for spherical ones. Because of the spherosymmetry of the problem, autofrettage in a spherical pressure vessel is treated as a one-dimensional problem and solved solely in terms of the radial displacement. The mathematical model is based on the idea of solving the elasto-plastic autofrettage problem using the form of the elastic solution. Substituting Hooke's equations into the equilibrium equation and using the strain-displacement relations, yields a differential equation, which is a function of the plastic strains. The plastic strains are determined using the Prandtl-Reuss flow rule and the differential equation is solved by the explicit finite difference method. The existing 2-D computer program, for the evaluation of hydrostatic autofrettage in a thick-walled cylinder, is adapted to handle the problem of spherical autofrettage. The presently obtained residual stress field is then validated against three existing solutions emphasizing the major role the material law plays in determining the autofrettage residual stress field. The new code is applied to a series of spherical pressure vessels yielding two major conclusions: The process of autofrettage increases considerably the maximum safe pressure that can be applied to the vessel. This beneficial effect can also be used to reduce the vessel's weight rather than to increase the allowable internal pressure. Secondly, the specific maximum safe pressure increases as the vessel becomes thinner. The present results clearly indicate that autofrettaging of spherical pressure vessels can be very advantageous in various applications Figure 5 shows the material behavior during the autofrettage process [4].

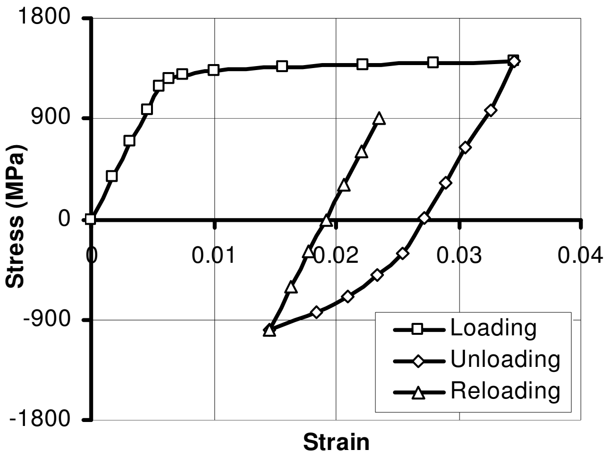

Figure 5: Material Behavior during the Autofrettage Process

Due to acute temperature gradients and repetitive high-pressure impulses, extremely dense internal surface cracks can be practically developed in highly pressurized thick-walled vessels, typically in gun barrels. In the authors' previous studies, networks of typical radial and longitudinal-coplanar, semi-elliptical, internal surface cracks have been investigated assuming both ideal and realistic full autofrettage residual stress fields. The aim of the present work is to extend the analysis two-fold: to include various levels of partially autofrettaged cylinders, as well as to consider configurations of closely and densely packed radial crack arrays. To accurately assess the stress intensity factors (SIFs), significant computational efforts and strategies are necessary, especially for networks with closely and densely packed cracks. This study focuses on the determination of the distributions along the crack fronts of K_{IP}, the stress intensity factor due to internal pressure, K_{IA}, the negative stress intensity factor resulting from the residual stress field due to ideal or realistic autofrettage, and K_{IN}, the combined SIF $K_{IN} = K_{IP} - |K_{IA}|$. The analysis is performed for over 1000 configurations of closely and densely packed semi-circular and semi-elliptical networked cracks affected by pressure and partial-to-full autofrettage levels of ε=30-100%, which is of practical benefit in autofrettaged thick-walled pressure vessels. The 3-D analysis is performed via the finite element (FE) method and the submodeling technique employing singular elements along the crack front and the various symmetries of the problem. The network cracks will include up to 128 equally spaced cracks in the radial direction; with relative, longitudinal crack spacing, 2c/d, from 0.1 to 0.99; autofrettage level of 30-100 percent; crack depth to wall thickness ratios, a/t, from 0.01 to 0.4; and, cracks with various ellipticities of crack depth to semi-crack length, a/c, from 0.2 to 2. The results clearly indicate that the combined SIFs are considerably influenced by the three-dimensionality of the problem and the Bauschinger effect. The Bauschinger Effect is found to have a dramatic effect on the prevailing combined stress intensity factors, resulting in a considerable reduction of the fatigue life of the pressure vessel. While the fatigue life can be finite for ideal autofrettage, it is normally finite for realistic autofrettage for the same crack network. Furthermore, it has been found that there are differences in the character of the SIFs between closely packed and densely packed crack networks, namely more dramatic drop-offs in KIA and KIN at the crack-inner bore interface for densely packed cracks further influenced by crack depth [5].

2.4 The Unexpected Behavior of Metals during "Shakedown" (A. Brot, IAI)

The "classical" *shakedown process* occurs when tensile stresses above the material yield strength are present at a notch, due to a large applied tensile stress. When these stresses are removed, *compressive residual stresses and tensile residual strains remain at the notch*. Under subsequent loading, the stresses at the notch are virtually elastic, and nearly all the plasticity effects have been *shaken-down*. The *compressive* residual stresses at the notch will thereby result in an increased fatigue life as a result of the classical shakedown process. Sometimes, the shakedown process is reversed, with large *compressive* stresses applied, resulting in *tensile* residual stresses. These tensile residual stresses are responsible for a *reduction in the fatigue life*.

There are documented cases reported in the literature, where aluminum and titanium upper wing skin structures, which perform in a compression dominated spectrum, have suffered fatigue failures [6] and [7]. Similarly, steel landing gear components have failed in fatigue, while their stress spectrum had primarily compressive loading [6].

This study analyzed several cases, using strain-life methodology, and showed that these unexpected results can be explained by the "shakedown" process. The analysis used the Ramberg-Osgood elastic-plastic *cyclic* stress-strain relationship together with the Neuber Equation to establish the expected local stress and strain excursions at a notch.

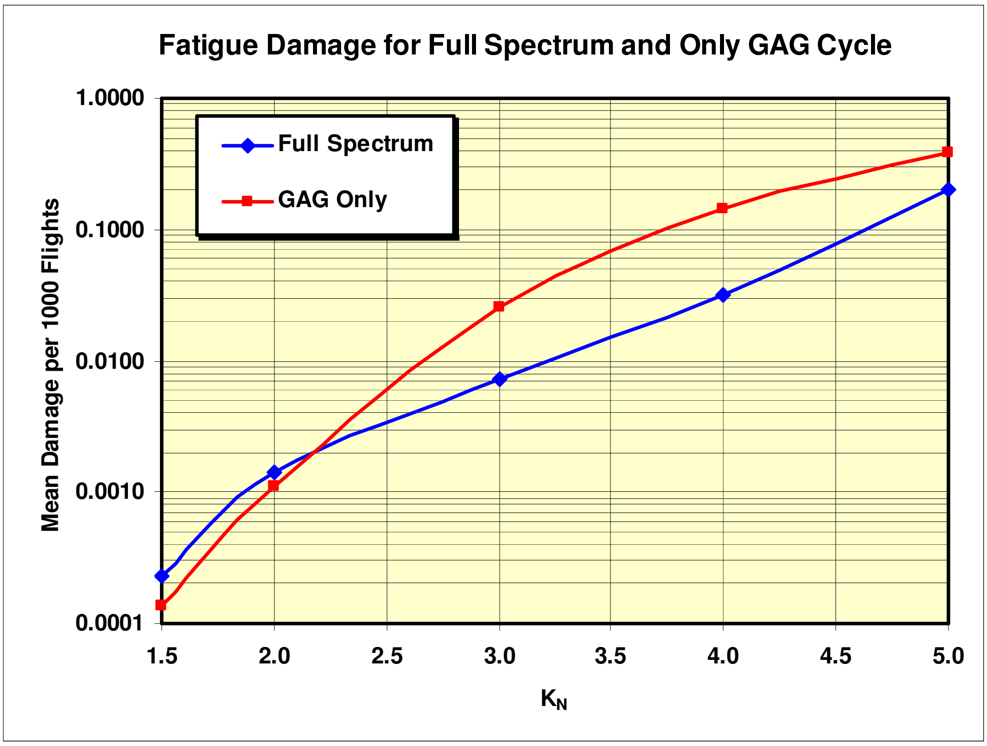

Figure 6: Damage per 1000 Flights on a Transport Aircraft Wing for the Two Gust Spectra

A strain-life fatigue analysis was performed for a 2024-T351 aluminum alloy lower wing skin of a transport aircraft subjected to gust loading. Under this gust loading, a maximum spectrum (nominal) stress of 29.2 ksi exists. The GAG cycle *(which is defined as the stress range, between loading in the air and on the ground, which occurs on the average, once-per-flight.)* is 18.5 ksi to -0.2 ksi. The strain-life analysis was performed for two spectra – The full gust spectrum described above and a spectrum consisting only of the GAG cycle. The results of these analyses are shown in Figure 6.

Figure 6 indicates, for K_N values above 2.2, the fatigue damage for the "GAG cycle" is *significantly greater* than that of the "full spectrum". The reason for this unexpected phenomenon is again due to the *shakedown process*.

The analysis showed that the compressive residual stresses arising from the “full spectrum” are far larger than those of the GAG cycles. These compressive stresses result in less fatigue damage for the “full spectrum” as compared to that for the "GAG cycle”.

These results were presented at the 50th Israel Annual Conference on Aerospace Sciences [8].

2.5 G150 Executive Jet Full-Scale Fatigue Test (A. Hermelin, IAI)

As part of the damage-tolerance certification, a G150 test-article was tested for two lifetimes (40,000 flights) of fatigue loading and another half-lifetime (10,000 flights) of damage-tolerance testing, where 24 artificial cracks were introduced. Testing was concluded with residual strength testing. This was accomplished successfully with a two-bay crack in the fuselage and large cracks by the access panels in both wings. This was reported in the 2009 Israel National Review [1].

The test-article included the fuselage and both wings. The tested areas consisted of the forward fuselage and cabin to the aft pressure bulkhead and fuel tank. Both entire wings were fatigue tested. Since the aft fuselage and empennage have not changed significantly from the G100 model, they were not fatigue tested and acted only as load application elements.

A selected teardown inspection (TDI) of the tested wing and the fuselage was started during January 2009 and was completed in June 2009.

A relatively small number of cracks were found on the fuselage and on the wing during the G150 full-scale test. Additional naturally developed cracks were found during the TDI of the test-article.

Several of these cracks were analyzed by means of a Scanning Electron Microscope. Basing on load-markers applied during the entire test, fractographic analyses produced crack growth time-history curves of the cracks, and enabled the estimation of the crack-initiation time for each of these cracks.

The results of the damage-tolerance testing and of the teardown inspection are being analyzed. All the cracks detected during the full-scale fatigue test (including the damage tolerance stage), and in the teardown inspection will be evaluated.

After the completion of this analysis, the G150 Continuing Airworthiness Report will be updated as needed, accounting for the crack findings and crack growth data measured during the full-scale fatigue test.

Figure 7 shows the disassembled cockpit and wing during the teardown inspection.

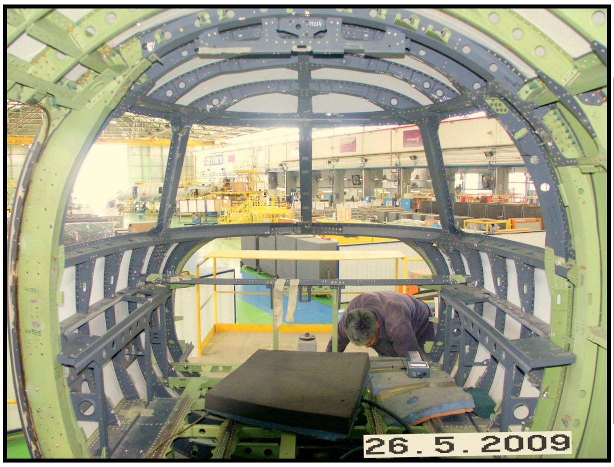

Figure 7: Disassembled Cockpit (left) and Disassembled Wing (right) for Teardown Inspection

2.6a G250 Executive Jet Fatigue Substantiation Program (Y. Peleg and Y. Freed, IAI)

This item was first reported at ICAF 2009 [1]. This report describes the current status of the project.

Israel Aerospace Industries and the Gulfstream Aerospace Corporation are currently jointly developing the G250 super mid-size executive jet. The aircraft will have a range of 3,400 nautical miles at a maximum speed of Mach 0.85. It will cruise at altitudes up to 45,000 feet. The first flight of the G250 took place during December 2009. Certification of the G250 to the FAA and EASA regulations is expected to be completed in 2011. Deliveries of the G250 will begin shortly after certification. The aircraft is powered by twin Honeywell HTF7250G engines, each producing 7,445 pounds of thrust. The G250 will be capable of nonstop flight from New York to London or from London to Dubai. The aircraft will have a very roomy and quiet cabin. The cabin environment will include 100% fresh air and a cabin altitude not exceeding 7,000 feet.

The Design Service Life Goal (DSLG) of the G250 is 20,000 flights or 36,000 flight-hours.

Figure 8 is a photo of a G250 Prototype Aircraft undergoing flight testing.

Figure 8: G250 Prototype Aircraft Undergoing Flight Testing

2.6b G250 Executive Jet Empennage (Z. Miller and A. David, IAI)

The G250 Empennage is a hybrid design, containing both aluminum and composite material structures. Figure 9 is a map of composite material usage on the G250 aircraft, showing the extensive use of composite materials on the empennage.

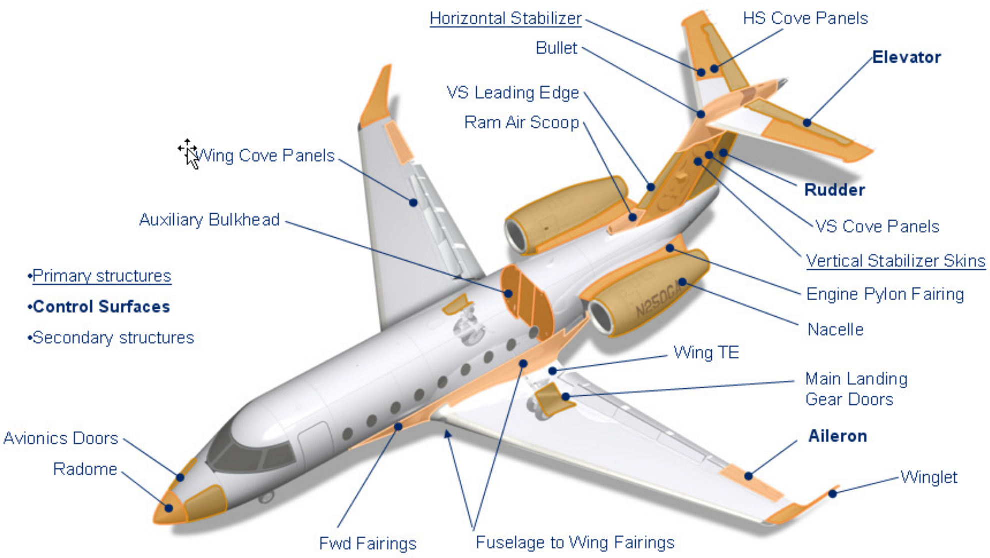

Figure 9: Map of Composite Material Usage on the G250 Aircraft

The G250 horizontal stabilizer consists of an aluminum inner torsion-box and a CFRP composite outer torsion box, as is shown in Figure 10. The elevator is a one-piece full-depth composite honeycomb structure.

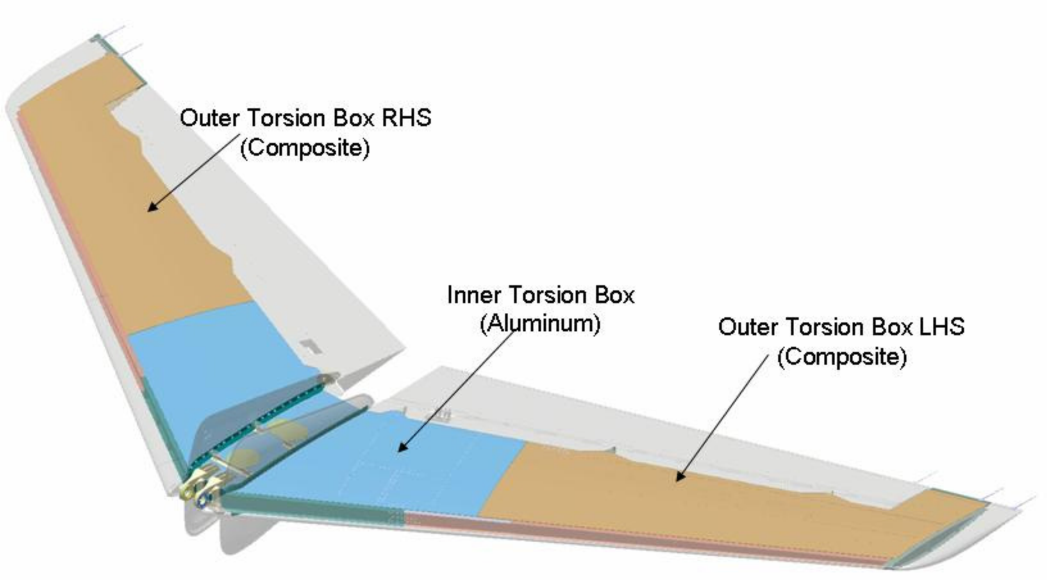

Figure 10: G250 Horizontal Stabilizer

The G250 vertical stabilizer consists of composite sandwich skins fastened to an aluminum substructure, as is shown in Figure 11. The composite material rudder is manufactured by RTM technology including a “one-shot” torsion box.

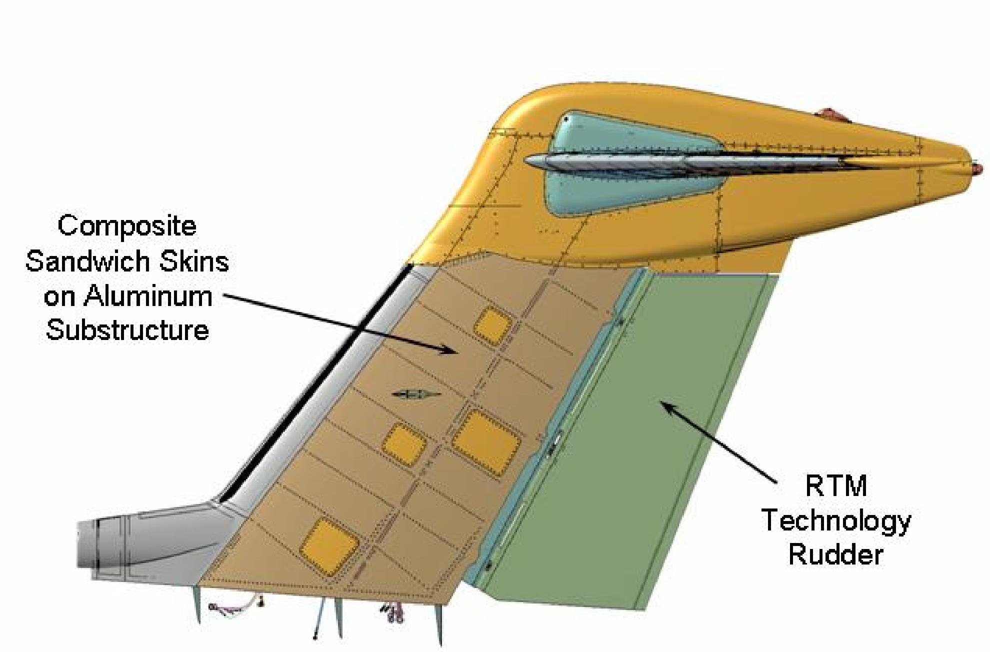

Figure 11: G250 Vertical Stabilizer

The metallic parts of the empennage were substantiated by damage-tolerance analysis, including the effects of thermal stresses that are generated due to the mismatch in the thermal expansion between the aluminum and the composite materials.

The composite material parts were substantiated based on the “no growth” philosophy. They have been shown to have adequate fatigue life due to the conservative strain levels used in the design. The composite material parts used for the full-scale fatigue test include *simulated manufacturing defects* and *barely-visible impact damage* (BVID) introduced at critical locations.

The empennage will be cycled, along with other parts of the aircraft, under flight-by-flight loading, for a duration of two lifetimes (40,000 flights). After completing the two lifetimes, the empennage will be tested with *clearly-visible impact damage* (CVID) for an additional 0.5 lifetime (10,000 flights). Finally, *ultimate loads* will be applied to certain empennage elements. *(See Section 2.6d for further details concerning the G250 full-scale fatigue test.)*

It is anticipated that the composite empennage critical locations will be first inspected in service *visually* at 10,000 flights and then at 5,000 flight intervals.

In order to support the structural substantiations, composite material elements were tested at extreme temperatures, and subcomponents were tested cyclically with loading up to 90% of the limit loads. Component tests are being performed for a vertical stabilizer torque-box and for an entire rudder assembly.

2.6c G250 Executive Jet, Rudder Fatigue Test (E. Eigenberg, IAI)

A fatigue test for the rudder assembly is being performed in order to verify the structural adequacy of the RTM manufacturing process, including the "one-shot" manufacturing of the torsion-box. The test-article was manufactured with *simulated manufacturing flaws* and *BVID* inflicted at critical locations. Figure 12 shows the rudder assembly test-article mounted to its fixture.

The first stage of testing consists of two lifetimes (40,000 flights) of spectrum loading. The spectrum loading includes load-enhancement and environmental factors, to account for scatter and environmental effects. The two-lifetime spectrum loading will then be followed by loading the structure to its *ultimate load*.

The second stage of testing will consist of increasing the damage at the critical locations to *CVID* proportions, and applying half a lifetime (10,000 flights) of spectrum loading. The purpose of this phase is to measure the damage growth at the critical locations. Following the half-lifetime of loading, the structure will be loaded to its *limit load*, thereby confirming its *residual strength capability*. All the damaged locations will then be repaired, and *ultimate loading* will be re-applied.

Figure 12: Fatigue Test of Entire Rudder Assembly

Strain-gage readings will be recorded every 2,000 flights and ultrasonic inspections will be performed at the same time. Testing has reached 20,000 flights (one lifetime) in March 2011.

2.6d G250 Executive Jet, Full-Scale Fatigue Testing (Y. Peleg, IAI)

As part of its damage-tolerance certification program, a structurally complete G250 test-article will be fatigue tested for two lifetimes (40,000 flights) followed by, approximately, half a lifetime (10,000 flights) of damage-tolerance testing, with artificial flaws inflicted at critical locations. Residual strength tests, under limit loads and cabin pressurization, will be performed in the presence of large cracks at several critical locations. This will be followed by a selected teardown inspection.

The test article consists of a structurally complete airframe, including the entire empennage structure. The vertical stabilizer, horizontal stabilizer, elevators, scissors, pivot fitting and dummy horizontal stabilizer trim actuator (HSTA) will be included in the fatigue test-article. Figure 13 shows the G250 fatigue test-article mounted in its loading fixture. Figure 14 shows a schematic view of the fatigue test setup, and showing the loading system.

Figure 13: Complete G250 Airframe Mounted in its Fixture and Ready for Fatigue Testing

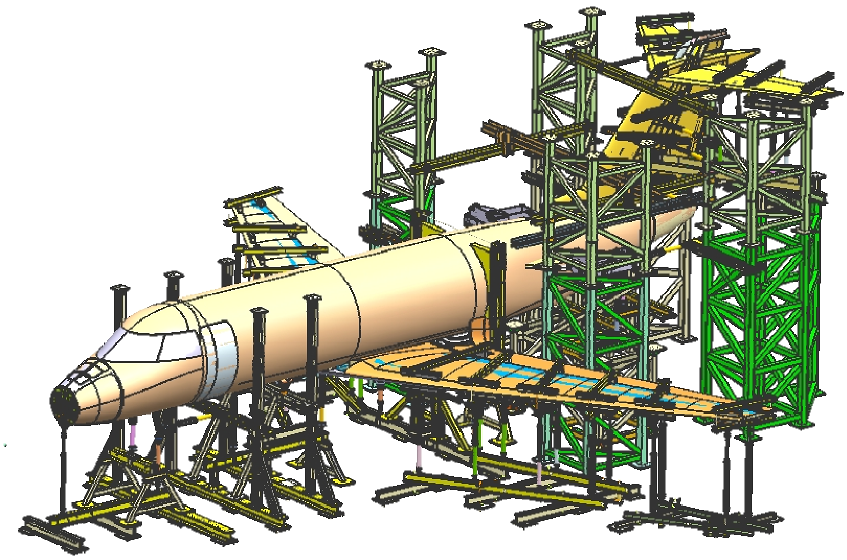

Figure 14: Schematic View of the G250 Fatigue Test Setup

The full-scale fatigue test spectrum will include a complete set of symmetric and asymmetric fatigue loads, including engine thrust reverser buffeting loading on the empennage and a suitable representation of engine support loading and main landing gear backup structure loading. The loading spectrum will contain 68 cycles per flight. Loads will be applied through 58 loading zones and will be reacted at six locations. A cabin pressure differential of 9.2 psi will be applied during each flight. Periodic inspection for cracks will be performed at suitable intervals using various NDI methods. Periodically, a total of 1364 strain-gage readings will be recorded, under a set of calibration loads, in order to determine if any significant fatigue damage has occurred at various critical locations.

At the end of two lifetimes (40,000 flights) of cyclic testing, artificial flaws will be introduced at several critical locations. The damage-tolerance test phase will be continued for another half a lifetime (10,000 flights), in order to ensure that sufficient crack growth data will be obtained. In addition to the artificial flaws, certain cracks detected during fatigue testing will not be repaired and their crack growth rates will be closely monitored during the damage-tolerance testing. Crack growth gages will be installed at crack tips to monitor the growing cracks until the end of the damage-tolerance phase of this test.

At the end of the cycling tests, a number of residual strength tests will be performed, including a two-bay crack in the fuselage. Some of the existing cracks will be enlarged significantly before the application of the residual strength loads

After the series of residual strength tests, two cases of ultimate load will be applied to the composite material horizontal stabilizer.

At the end of the fatigue test, a selected teardown inspection will be performed, where selected areas of the test-article will be disassembled and inspected for cracks.

The full-scale fatigue test is scheduled to begin very shortly and will continue for several years.

In addition to the full-scale fatigue test described above, fatigue and damage-tolerance component tests will be performed for the main landing gear, aileron (composite material), spoiler, and flap extension system.

2.6e G250 Executive Jet, Main Landing Gear (MLG) Fatigue Test (Y. Peleg, IAI)

The fatigue test spectrum of the G250 MLG consists of ten blocks, each representing a half-lifetime of the landing gear – 10,000 flights. Testing is planned to reach 100,000 flights, which corresponds to five lifetimes.

Each 10,000 flight block is divided into two phases. During the first phase, the landing gear will be loaded first in its extended ("down and locked") position. Flight-by-flight, vertical, drag and side ground loads, simulating 10,000 flights (taxiing, turning, braking, take-off and landing), are applied. Approximately 13.5 cycles per flight are applied.

After completion of the first phase, the landing gear will be re-installed in its retracted position. In this position, the Side Brace will be subjected to 12,000 load cycles while simulating in-flight loading of the gear in its "Up" position. *(The 12,000 cycles account for normal operation + additional maintenance retract / extend cycles.)*

27 strain gages were bonded to the test specimen, to monitor possible stress changes during progress of the fatigue test.

After each block (10,000 ground / 12,000 retraction-extension load cycles), the landing gear will be inspected for cracks and for wear. After the completion of each lifetime (20,000 flights), the landing gear will be removed from the test rig, and disassembled. Major parts of the gear will be inspected by NDT, and dimensional checks of significant parts will be performed. After the inspection, the landing gear will be re-assembled and installed for the next fatigue test block, until all ten blocks are completed, signifying five lifetimes of fatigue testing.

Figures 15 and 16 show the G250 MLG fatigue test setup. Main landing gear fatigue testing has reached 20,000 flights (one lifetime) in March 2011.

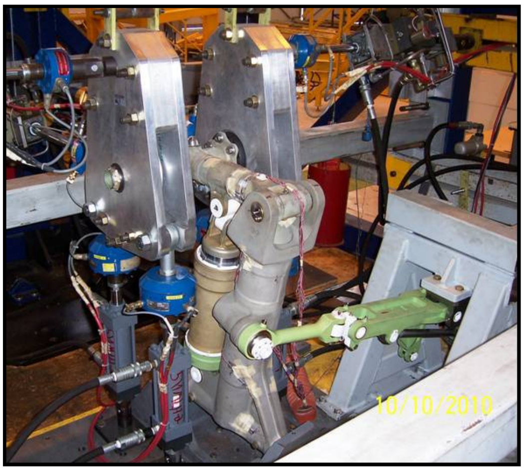

Figure 15: G250 Main Landing Gear Fatigue Testing

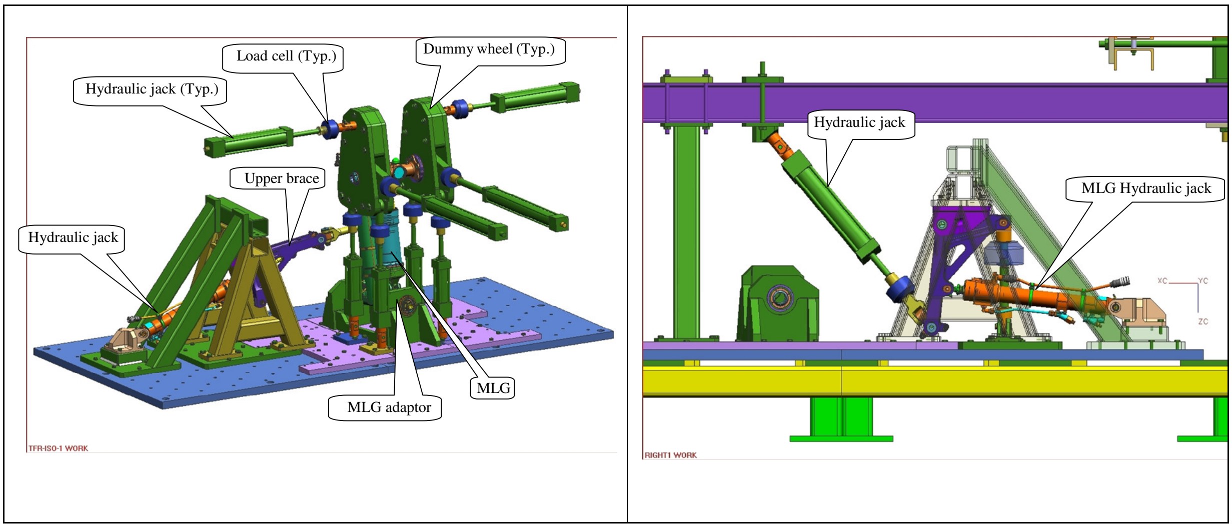

Figure 16: G250 MLG in its Extended *(left)* and Retracted *(right)* Configurations

3 STRUCTURAL INTEGRITY OF COMPOSITE MATERIALS

3.1 Use of Accelerated Testing Methodology to Obtain Static and Fatigue Properties of Unidirectional Composite Materials (Y. Freed, IAI)

This activity was performed in cooperation with S. Rzepka of Fraunhofer ENAS, Germany under the framework of the “Clean Sky” project with partial funding from the European Commission.

With the increase use of unidirectional composite materials as primary structures in advanced light-weight aerospace products, the ability to predict long term behavior of composite materials becomes essential. Since these products are designed to a target life-goal of several dozens of years, it is needed to establish an accelerating testing methodology than can replace a long term real-time testing.

In this study, an accelerated testing methodology is introduced. This method was originally designed for non-destructive material properties, but it can be shown that it may be applicable to certain types of composite materials as well. The basic idea of this method is to perform viscoelastic testing at several elevated temperature states to obtain a relation between the temperature and the testing time periods. This relation, usually referred to as a 'time-temperature superposition principle' (TTSP), holds for creep, residual strength, and fatigue behavior of the composite material. With additional sets of simple constant strain rate and fatigue coupon tests, the degradation of the mechanical properties of the composite material, upon applied cyclic loading over long term periods in standard operational temperatures, can be determined. This procedure is schematically described in Figure 17.

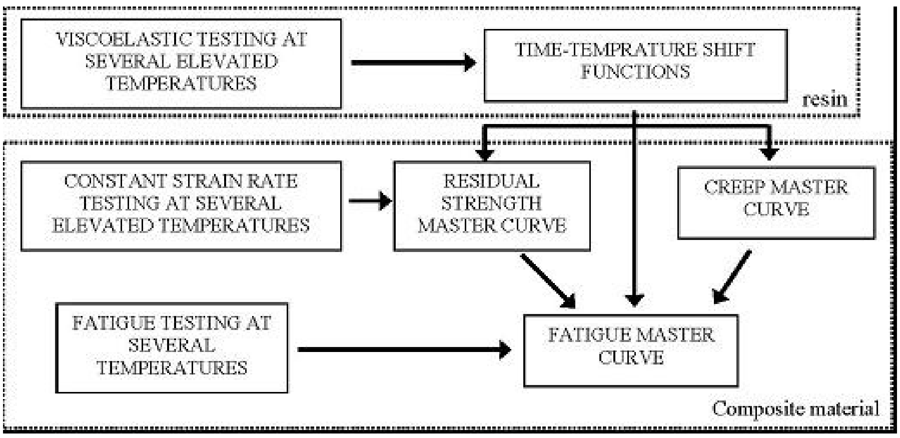

Figure 17: Schematic Description of the Accelerated Testing Methodology

The outcome of the procedure described above is a set of master-curves, in which the long term behavior of the composite material is described in terms of applied loads, number of cycles to failure, load frequencies, and operational temperatures. This is an efficient and systematic approach to life prediction, since only one fatigue master curve is needed to predict the lifetime of the composite material at any load frequency or elevated temperature. Since this simple coupon testing is performed in short time durations, it significantly reduces the overall testing time (by approximately 99%), as compared to real-time testing along the product design life; hence the term 'accelerating testing'. Since the accelerating testing minimizes the test durations, a significant reduction of energy consumption is achieved as well as reduced environmental impact.

This study focuses on the prediction of long term residual strength, creep and fatigue characteristics of T300/913 unidirectional composite material. Both three point bending and tensile specimens were tested. The relation between time and temperature was establishes, and residual strength, creep and fatigue master-curves were determined. These curves were compared to test results at different elevated temperatures, applied strain rates and cyclic loading frequencies. From the preliminary results, it can be readily concluded that the time-temperature superposition principle indeed holds for creep, residual strength and fatigue behavior of the T300/913 unidirectional tape. Our next goal is to assess the effect of water absorption due to moisture on the residual strength and fatigue behavior of the unidirectional tape. A similar methodology with time-temperature-moisture relation will assist in determining the long term response of the composite material under any temperature and moisture environmental conditions. Typical results are shown in Figure 18.

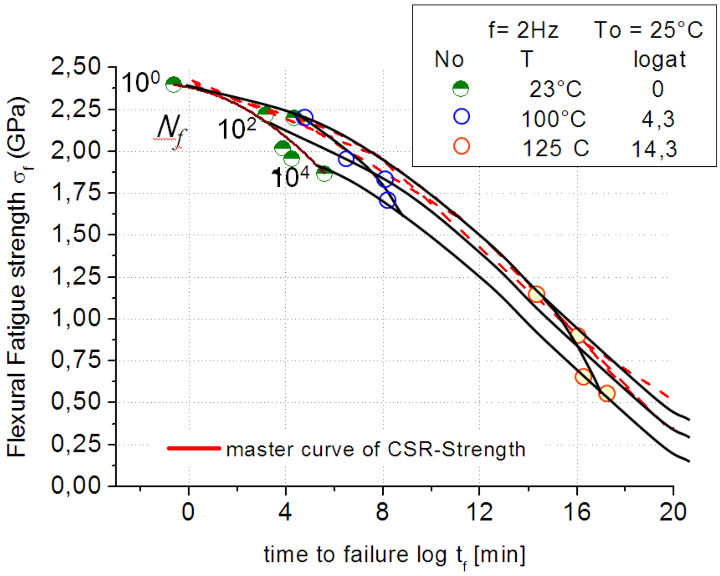

Figure 18: Fatigue Master Curve Obtained by Testing at Different Loads and Temperatures

From the results presented in this paper, it was concluded that the time-temperature superposition principle indeed holds for creep, residual strength and fatigue behavior of the T300/913 unidirectional tape. The results of this study will be presented at the 26th ICAF Symposium [9].

3.2 Health and Usage Monitoring of Composite UAV Structures Using Fiber-Optic Sensors (I. Kressel, IAI, M.Tur, TAU and S. Gali, Consultant)

This work was performed in cooperation between Israel Aerospace Industries, Tel-Aviv University, the Aeronautical Development Establishment (Bangalore, India) and the National Aerospace Laboratories (Bangalore, India).

The high maneuverability and harsh launch and landing conditions of modern Unmanned Aerial Vehicles (UAVs), demand constant monitoring of their structural airworthiness. The recently introduced Health and Usage Monitoring Systems (HUMS) concept, aims towards effective real-time assessment of the structural integrity of flying vehicles, should provide a practical mean of maintaining structural airworthiness at a minimal cost. This is highly important for composite-made UAVs, where conventional inspection methods of valuable structural components are stymied due to limited accessibility.

Fiber optic sensors, in particular Fiber Bragg Grating sensors (FBG), appear to be excellent candidates to be used in SHM applications due to their high sensitivity to mechanical strain, small size, immunity to electrical interference, low weight, long life, durability under extreme environmental conditions, and capability of high speed sensing and dense multiplexing. Moreover, for composite structures, these sensors can be easily embedded into the structure during manufacturing, eliminating the need for sensor protection. An advanced smart load monitoring system for a UAV composite tail boom, based on an array of FBG sensors was built and tested. The FBGs are used for direct static and dynamic loads evaluation of the Nishant UAV tail booms during all flight stages, including take-off and landing. The system is designed to collect data during actual flights. In order to meet this challenging requirements, a solid state, high sampling rate (>2kHz) FBG interrogation unit is used, capable of tracking multiple fibers, having multiple FBGs on each. The optical fibers are polyimide-coated to assure good bonding to the composite structure.

Figure 19 shows the *Nishant* UAV which was designed and manufactured in India.

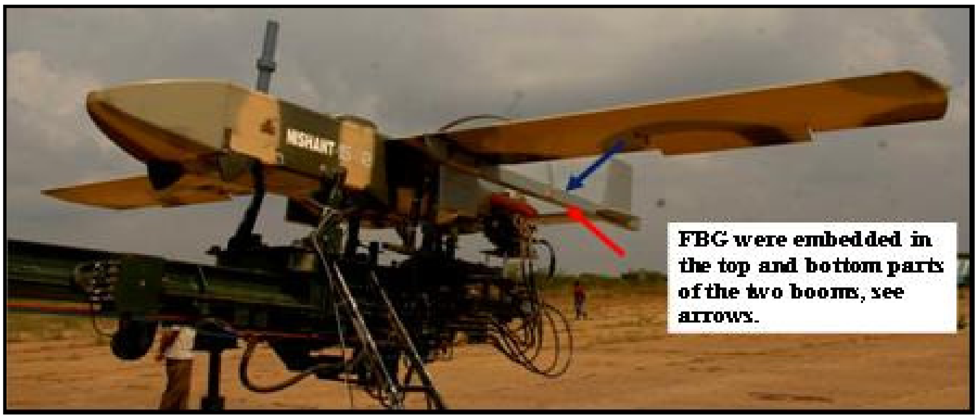

Figure 19: The *Nishant* UAV on its launcher

The FBG sensor net, comprising 4 fibers, each with 4 sensors per boom, was tailored to monitor critical locations in the boom, based on a detailed finite element analysis. The gathered information from the 16 sensors was fused, following noise reduction and spectral analysis. Figure 20 shows a calibration test of the FBG sensors mounted to a boom.

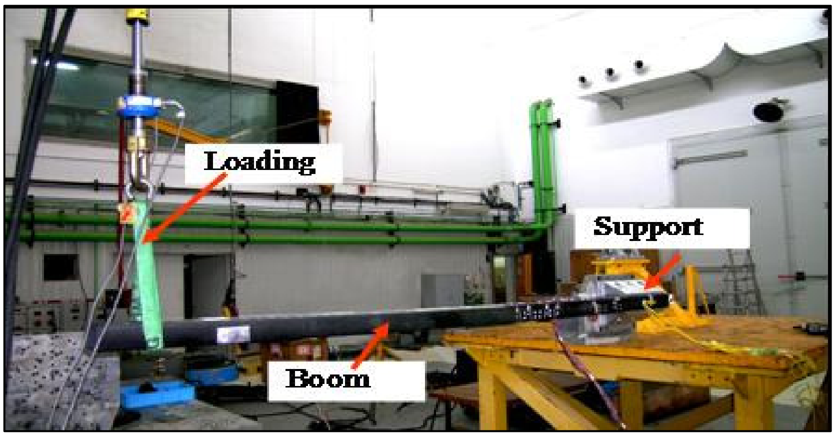

Figure 20: UAV Boom Calibration Test of FBG Sensors

The system was first tested on ground by subjecting the UAV booms to both static, impact and vibration loading, simulating real flight conditions (including engine runs up to maximum RPM). It was demonstrated that the system could track the development of very small strains (~10με) in the booms, making it possible to identify all major natural frequencies and mode shapes. Comparison of the FBG readings with a conversional tracking system results, based on strain gages and accelerometers, showed excellent agreement. It was demonstrated that the FBG readings can track the real boom state in real time.

Figure 21 shows typical FBG sensor strain readings during the launch and parachute recovery stages of flight.

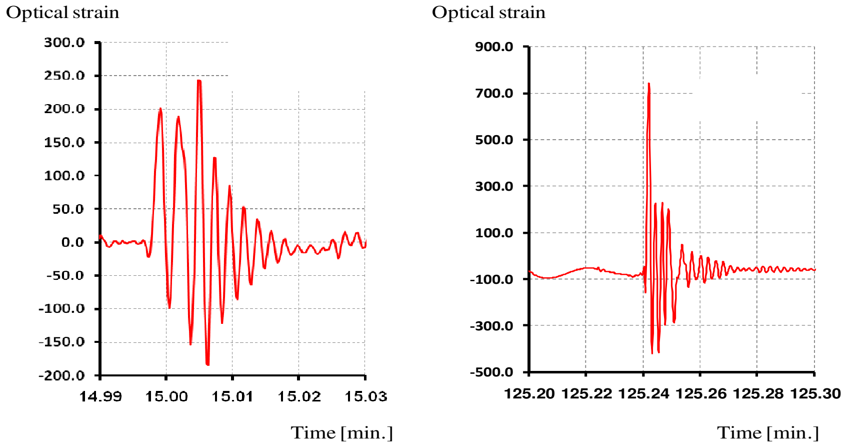

Figure 21: Typical FBG Sensor Readings During Launch *(left)* and Parachute Recovery *(right)*

By utilizing this highly promising, fiber optic sensor based interrogation concept, airworthiness deterioration may now be monitored in real time, reducing maintenance costs and increasing the availability of such UAVs.

A summary of this activity will be presented at the 26th ICAF Symposium [10].

3.3 Health and Usage Monitoring of a Cobra Helicopter Structure (I. Kressel, IAI and N. Shemesh, IAF)

This activity is a continuation of previous work presented in the 2009 Israel National Review on the subject of the analysis and testing of bonded composite patch repairs [1].

Figure 22: Cobra AH-1S Assault Helicopter

Cracks were found on the aluminum honeycomb skins of the vertical fin in *most* of the IAF fleet of the AH-1S Cobra assault helicopter (Figure 22). The standard metallic repair did not solve the problem, and several tails had to be replaced. A composite material patch was developed to prevent future cracking of the fin and to retard the crack growth on cracked fins. Analytical and experimental measurements have shown that the composite material patch is very effective in solving this problem.

A Fiber-Bragg-Grating (FBG) based advanced Health and Usage Monitoring sensing net, imbedded in a co-cured composite patch repair, was proposed and demonstrated. Vibration loads, patch debonding and crack propagation rate were monitored using a low spatial resolution Fiber-Bragg-Grating sensor net embedded in the composite patch. Measurements are taken of changes in the strain field induced by thermal mismatch between the composite patch and the metal substrate. The strain field in the composite patch is affected by both a growing crack in the metal substrate and patch-to-substrate debonds. By correlating these strain measurements with a numerical model, this sensing concept is able to identify and track damage propagation during service with a spatial resolution much better than that of the sensor net.

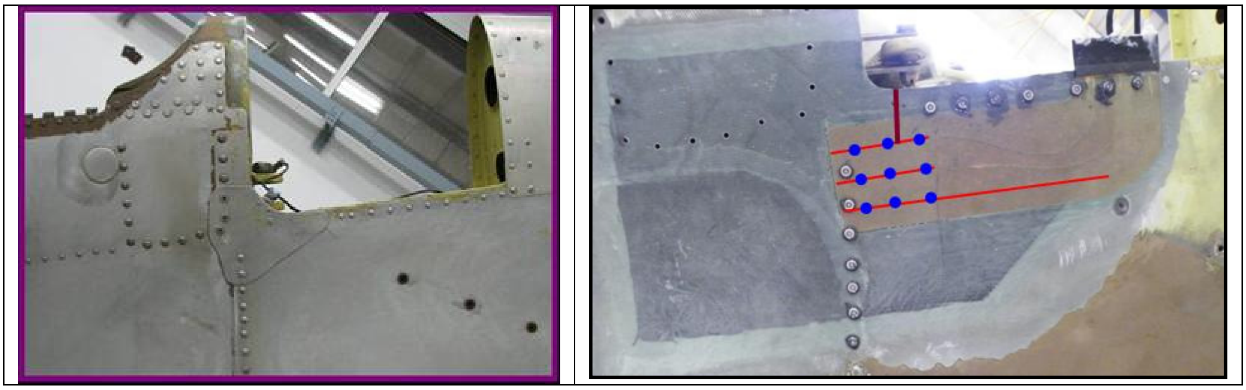

Figure 23: *Standard* Metallic Repair of Vertical Fin *(left)* and *Smart Composite* Repair *(right)*

Figure 23 shows both the *standard* metallic repair and the *smart* composite repair. *(The embedded sensors are seen in Figure 23.)* The concept of using bonded composite repairs for the maintenance of aging metallic aircraft has been proven both as a preventive measure and as a method for retarding future growth of existing damage. The main advantages of a bonded repair as compared to a metallic bolted one, are its smoother load transfer, the elimination of stress concentration due to additional fasteners, the good fatigue and damage-tolerance behavior of the composite patch and its easy application on curved areas. One of the disadvantages of bonded composite repairs is the lack of non-destructive means for structural integrity assessment during the application and service of such repairs. Presently, most commercial inspection procedures for bonded composite structures, including bonded repairs, are based on detecting voids using ultrasonic techniques at scheduled maintenance intervals. Since in many cases a structural defect may not be associated with a void, ultrasonic inspection may be ineffective leading to incorrect structural integrity assessment.

The recently introduced smart repair concept is aimed towards real-time assessment of repair integrity based on direct monitoring of internal strains, using embedded sensors. Repair degradation may now be predicted before delamination or debonding can by detected by ultrasonic techniques.

This work presents experimental and numerical evaluation of an advanced co-cured smart composite patch repair applied on an IAF helicopter tail, based on an embedded, low spatial resolution, optical Fiber Bragg Grating sensor net. The FBG readings combined with numerical predictions are used for direct assessment of repair integrity during service. Figure 24 shows the FEM calculated stress-intensity of a crack in the fin for various repair schemes, thereby demonstrating the effectiveness of the patch repair.

The results of this study were presented at the 51st Israel Annual Conference on Aerospace Sciences [11].

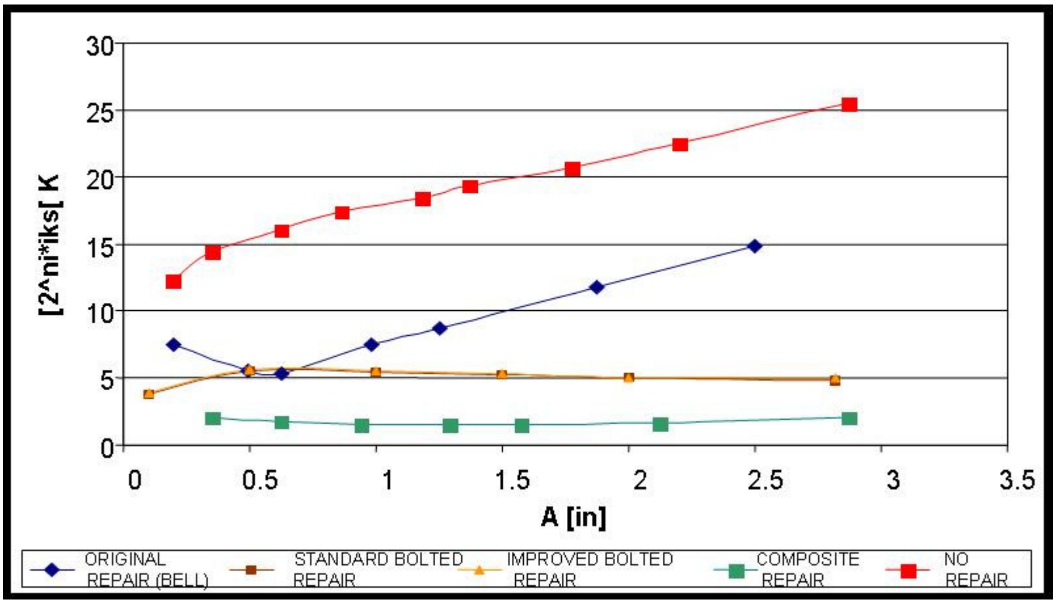

Figure 24: FEM Calculated Stress-Intensity of a Fin Crack for Various Repair Schemes

4 PROBALISTIC STUDIES

4.1 Substantiating Fatigue Lives of Structures by Using a Weibayes Distribution, (A. Brot, IAI)

The Weibull distribution is a very versatile statistical distribution that has been used to establish an allowable fatigue life from the service life history of several specimens or components.

The Weibull statistical distribution generally has two unknown parameters, the "characteristic life" (η) and the "shape-factor" (β). Often, it is assumed that the shape-factor is a known parameter, for example, as a function of the specific material or alloy. Many experimental investigations have been performed that show that $\beta \cong 4$ for aluminum structures and $\beta \cong 3$ for titanium and moderate strength steel. It should be noted that a large value of the shape-factor corresponds to little scatter of results, while a small value implies much scatter.

When a Weibull analysis is performed under the assumption that the shape-factor is *a priori* known, this is sometimes called a ***"Weibayes Analysis"***. A more precise name for this procedure is a one-parameter *Weibull analysis (using an assumed shape-factor).* Making this assumption greatly simplifies the analysis, but the assumption of a known shape-factor must be verified by testing or be taken from valid "historical failure data". In a Weibayes analysis, where the shape-factor (β) is assumed to be known, the characteristic life (η) can be easily determined from a series of fatigue tests.

If sufficient fleet data exists and a fatigue test (to another spectrum) may have been performed in the past, a statistical analysis can be performed, using this Weibayes procedure, to determine the maximum expected probability of failure. If the probably of failure is shown to be very low over the design lifetime, it *may* be possible to substantiate the component without performing an additional fatigue test.

One may ask, if we have test data on the failures of several specimens, why not perform a two-parameter Weibull analysis with the data? The resulting values of η and β can then be used to determine the probability of failure at any design life.

The answer lies with achieving a reasonable confidence level. If we require a 95% (lower) confidence level, 15 to 20 specimens may be required to achieve a reasonable probability of failure, when using the two-parameter Weibull analysis. On the other hand, a Weibayes analysis, using an assumed value of shape-factor (β), can result in reasonable results even while using as few as 3 to 5 specimens. *(This is due to the large sensitivity of the Weibull solution to possible variations in the shape-factor, when dealing with a small number of specimens. On the other hand, the Weibayes solution, which does not allow for variation in the shape-factor, is far less sensitive.)*

Figure 25 describes a Weibull and a Weibayes distribution for a seven-specimen fatigue test. If a 95% lower confidence level is required, it is clear from Figure 25 that the Weibayes distribution is more useful.

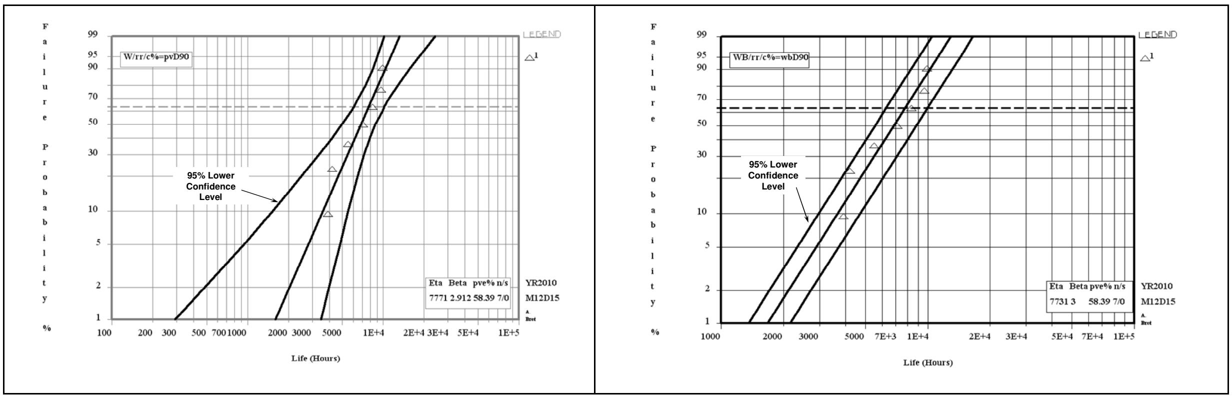

Figure 25: Weibull (left) and Weibayes (right) Distributions for a Seven-Specimen Fatigue Test

Weibull and Weibayes statistical distribution methodology was developed to determine the expected probabilities of failure of aircraft components that will operate under a severe fatigue spectrum. A landing gear application was investigated to determine whether a Weibayes analysis could be used in lieu of a five-lifetime fatigue test.

This study was presented at the 51st Israel Annual Conference on Aerospace Sciences [12].

5 MISCELLANEOUS

5.1 Edge and Vertex Singularities in Structures (Z. Yosibash, Ben-Gurion University)

This research is a continuation of previous work presented in the 2009 Israel National Review [1].

The computation of eigen-pairs and generalized stress intensity factors in the vicinity of singular points as well as the thermal stress intensity functions in 2-D domains, and their relation to failure initiation is extremely important in engineering practice. Much interest is also devoted to 3-D domains where edge and vertex singularities are present and edge stress intensity functions (ESIFs) in the neighborhood of edges have major importance in engineering practice. These topics are being presented in detail, with many examples from engineering practice, in a new book by Z. Yosibash that is scheduled to appear in 2011 [13].

Elasticity problems having edge and vertex singularities in three-dimensional (3-D) domains have been also investigated recently by Z. Yosibash and collaborators [14, 15].

In [Y] we address the solution $u(\rho,\theta,\varphi)$ to the Laplace equation in the neighborhood of a vertex in a three-dimensional domain, which may be described by an asymptotic series in terms of spherical coordinates $u=\sum_i A_i \rho^{\alpha_i} f_i(\theta,\varphi)$. For conical vertices we derived explicit analytical expressions for the eigen-pairs α_i and $f_i(\theta,\varphi)$ which are required as benchmark solutions for the verification of numerical methods. We also extended the modified Steklov eigen-formulation for the computation of vertex eigen-pairs using p/spectral finite element methods, and demonstrated its accuracy and high efficiency by comparing the numerically computed eigen-pairs to the analytical ones. Vertices at the intersection of a crack front and a free surface were also considered and numerical eigen-pairs are provided. The numerical examples demonstrate the efficiency, robustness and high accuracy of the proposed method, hence its potential extension to elasticity problems.

In [15] we derived the asymptotics of solutions to the Laplace equation with Neumann or Dirichlet conditions in the vicinity of a circular singular edge in a three-dimensional domain and are provided in an explicit form. These asymptotic solutions are represented by a family of eigen-functions with their shadows, and the associated edge flux intensity functions (EFIFs), which are functions along the circular edge. We provided explicit formulas for a penny-shaped crack for an axisymmetric case as well as a case in which the loading is nonaxisymmetric.

Explicit formulas for other singular circular edges such as a circumferential crack, an external crack and a 3π/2 reentrant corner are also derived. The mathematical machinery developed in the framework of the Laplace operator was extended to derive the asymptotic solution (three-component displacement vector) for the elasticity system in the vicinity of a circular edge in a three-dimensional domain. As a particular case we presented explicitly the series expansion for a traction free or clamped penny-shaped crack in an axisymmetric or a non-axisymmetric situation.
The precise representation of the asymptotic series is required for constructing benchmark problems with analytical solutions against which numerical methods can be assessed, and to develop new extraction techniques for the edge flux/intensity functions which are of practical engineering importance in predicting crack propagation.

5.2 TaxiBot – A New Concept for "Smart" Dispatch Towing (A. Perry and A. Hermelin, IAI)

This topic was first reported in 2009 [1]. Since then, there have been several *exciting developments*.

Since the start of the widespread use of towbarless towing, there have been many suggestions/attempts to tow aircraft directly from the gate to the takeoff runway (dispatch towing) in order to save fuel and reduce pollution. In the past, these proposals have all been dismissed by the airframe manufacturers due to the expected reduction of the fatigue life of the nose landing gear, due to the many towing load cycles that will be applied during dispatch towing [16].

Nevertheless, the dispatch towing concept has many advantages. A study has shown that an annual savings of \$7.3 billion of fuel expenses and 23 million tons of CO_2 emission can be realized, if all wide-body and narrow-body aircraft are towed to their takeoff points. *(A large wide-body aircraft burns about 355 gallons of fuel for every 17 minutes of taxi-out time needed to reach its takeoff point.)*

IAI, together with Airbus and other subcontractors, has developed a semi-robotic towbarless towing vehicle called TaxiBot. Under this concept, the pilot of the aircraft remains in full command during the entire TaxiBot towing process, in contrast with the regular dispatch towing (where the driver is in control). In order to slow down, the pilot will apply the aircraft brakes (on the main landing gears) as needed, thereby reducing the number and magnitude of load cycles applied to the nose gear by the *airplane-to-tug* mass ratio (10 for wide-body airplanes). The airplane engines will be started-up only shortly before takeoff, thereby saving fuel and reducing pollutants.

The TaxiBot control system will be designed to limit the magnitude of loads that can be applied to the nose gear, thereby controlling the towing traction force envelope accordingly. This concept has been proved during instrumented TaxiBot testing. Test measurements have confirmed that TaxiBot towing will not result in any reduction of the nose landing gear fatigue life.

In coordination with Airbus, a TaxiBot towing demonstration was held between March and June 2010 in Toulouse on an instrumented Airbus A340-600 aircraft. The purpose of this demonstration was to verify the operational performance of the TaxiBot and to confirm that the TaxiBot towing load spectrum is not more severe than the spectrum to which the nose landing gear of the aircraft was certified to. Figure 26 shows the TaxiBot demonstrator towing the Airbus A340-600 aircraft.

Figure 26: Airbus A340-600 Towed by the TaxiBot Demonstrator at Toulouse Airport

In coordination with Lufthansa LEOS, a Boeing B747-400 aircraft was towed very successfully at Frankfurt Airport on 27-28 December 2010 under severe weather conditions (snow and ice) at a temperature of -17°C. TaxiBot towed the airplane within the predetermined NLG load envelope. Lufthansa has expressed a desire to begin TaxiBot operations by the end of 2012, probably in Munich Airport.

Figure 27 shows the TaxiBot demonstrator towing the Boeing B747-400 aircraft.

Figure 27: Boeing B747-400 Towed by the TaxiBot Demonstrator at Frankfurt Airport

5.3 Progress at the Dreszer Fracture Mechanics Laboratory (L. Banks-Sills, Tel Aviv University)

During the last two years, characterization of the behavior of interface cracks between isotropic materials and fiber reinforced, laminate composite material has been continuing. In addition, we are currently considering the fracture behavior of an interface crack between woven layers in different directions

A graduate student, Konovalov [17] and an undergraduate student, Fliesheer [18] carried out three-dimensional analyses on bimaterial Brazilian disk specimens (see Fig. 29). In Fig. 29a, a glass/epoxy specimen is shown with a 1 mm thick aluminum (AA 2024-T851) ring surrounding the epoxy. The ring was added to induce compressive stresses at the specimen edges to prevent separation. In Fig. 29b, two ceramic clays, K-142 and K-144, (Vingerling, Holland) were bonded together. In each case, there is a central crack of length 2a along the interface. The nominal radius and thickness of the specimens are R and B, respectively. Various mixed mode combinations are attained by rotating the specimen within the loading frame, that is, changing the angle ω. Twenty-five glass/epoxy specimens were tested and presented in Banks-Sills et al. [19]; thirty-one bimaterial ceramic clay specimens were tested and presented in Banks-Sills et al. [20]. In both cases, the specimens were analyzed assuming two-dimensional deformation. Konovalov [17] and Fliesher [18] each considered one of two material pairs carrying out three-dimensional analyses to assess its effect on the results. The glass/epoxy specimens in Fig. 29a were examined by Konovalov [17] in which she developed all of the software related to the interaction energy integral necessary for the analyses. Using this software, Fliesher analyzed the specimen shown in Fig. 29b composed of the two ceramic clays. As a result of their studies, this investigation was presented at ICF12 in Ottawa [21] and a paper was published in the International Journal of Structural Integrity [22].

It would appear from the results obtained that for a body containing an interface crack which is subjected to in-plane loading, it is sufficient to use a two-dimensional approach to analyze failure. Of course, the three-dimensional failure surfaces and approach presented in that paper may be used in a case for which the applied load is three-dimensional. From an engineering approach, it might even be sufficient to determine G_{1c} by means of two-dimensional testing and analyses, and use it in three dimensions, with a safety factor.

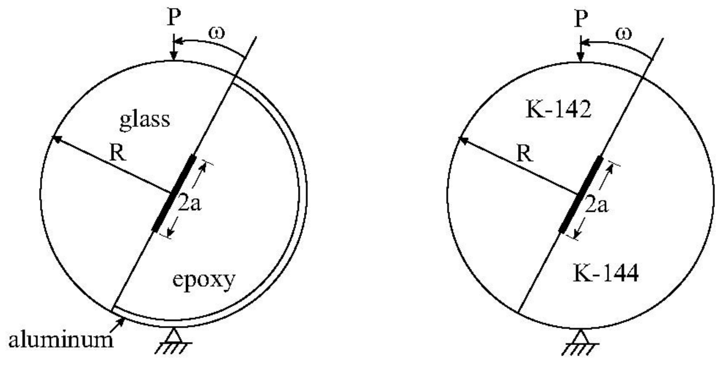

(a) (b)

Figure 29: Brazilian disk specimen composed of (a) glass and epoxy and (b) two ceramic clays.

Delaminations in laminated composites have been considered between a number of different interfaces. Most recently, an M.Sc. student, Liran Rogel considered the +30°/ − 60° and −30°/60° interfaces [23, 24]. For example, for the +30°/ − 60° interface, the fibers of the composite of the upper material are rotated 30° in the clockwise direction with respect to the x_1-direction (see Fig. 30a), whereas the fibers in the lower material are rotated 60° in the counter-clockwise direction (see Fig. 30b). The second material pair is defined in a similar manner. The delamination is situated in the $x_1 - x_3$ plane (see Fig. 31) with the x_3-axis along the delamination front and the x_2-axis perpendicular to the delamination faces.

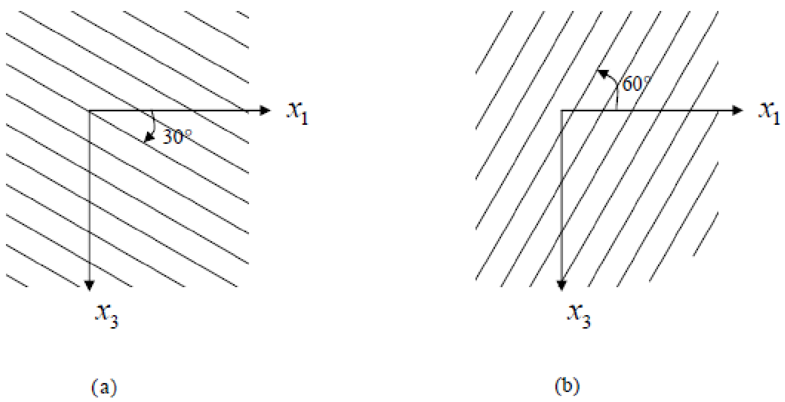

Figure 30: Fiber direction in (a) upper material, and (b) lower material for the +30° / − 60° interface.

In this investigation, the asymptotic fields for the +30°/ −60° and −30°/60° interfaces were developed. In these cases, as well as most others, there are five stress intensity factors, namely K_1, K_2 and K_3 associated with the square-root, oscillatory singularity and two stress intensity factors, K_{II} and K_{III} , associated with the square-root singularity. It was found, however, that there is a relation between K_2 and K_3, as well as between K_{II} and K_{III}. This study was presented at two conferences [25, 26]. These studies are leading up to an investigation of a penny-shaped crack in a cross-ply.

Various expressions are used in the literature for the stress-intensity factors of interface cracks between anisotropic material. In particular, two of these approaches were discussed and compared for orthotropic and monoclinic materials [27. Relations between the stress-intensity factors were found. Expressions for the interface energy release rate G_i were presented. Although the expressions appear different, they are shown to be the same by using the relations between the stress-intensity factors. Phase angles were defined which may be used in a fracture criterion.

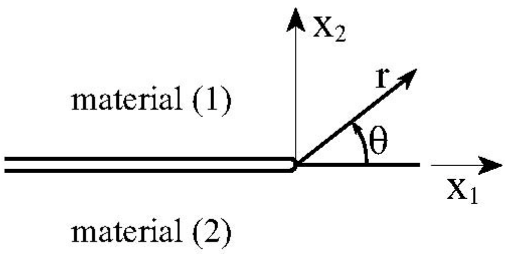

Figure 31: Delamination front coordinates

Studies on the cracking of piezoelectric materials have continued. There are four intensity factors for cracks in piezoelectric materials: the usual stress intensity factors for the three modes of deformation K_I, K_{II} and K_{III} and a fourth intensity factor K_{IV} related to the electric flux density vector D_i. Fracture tests were carried out on unpoled and poled PZT-5H four-point bend specimens [28, 29 and 30]. The crack faces were taken parallel to the poling direction. Both mechanical loads and electric fields were applied to the poled specimens. The experimental results were analyzed by means of the finite-element method and a conservative M-integral including the crack face boundary conditions. Fracture tests on four point bend PIC-151 specimens, with the crack faces perpendicular to the poling directions, were also analyzed in those studies; the experimental results were taken from the literature. A mixed-mode fracture criterion was proposed for piezoelectric ceramics. This criterion is based upon the energy release rate and two phase angles. This criterion was implemented with experimental results from the literature and from this investigation. Excellent agreement was found between the fracture curve and the experimental results of the specimens with the crack faces perpendicular to the poling direction. With some scatter, reasonable agreement was observed between the fracture curve and the experimental results of the specimens with crack faces parallel to the poling direction. Some of this work was presented at the Second Broberg Conference in Sweden [31].

To address the problem with the scatter obtained when the crack is parallel to the poling directions, a further set of tests were carried out on PVT-5H [32]. An improved method was used for inducing the cracks. In addition, the M-integral was refined for this application. Better agreement was found between the experimental results and the fracture curve. These results were presented at the Israel Society for Theoretical and Applied Mechanics [33].

Finally, a review paper was published [34] in which the problem of calculating stress-intensity factors in two-and three-dimensional mixed-mode problems, was considered for isotropic and anisotropic materials. The square-root singular stresses in the neighborhood of the crack tip were modeled by quarter-point, square and collapsed, triangular elements for two-dimensional problems, respectively, and by brick and collapsed, prismatic elements in three dimensions. The stress-intensity factors were obtained by means of the interaction energy or M-integral. Displacement extrapolation was employed as a check on the results. In addition, the problem of interface cracks between homogeneous, isotropic, and anisotropic materials was presented. The purpose of this paper was to present an accurate and efficient method for calculating stress-intensity factors for mixed-mode deformation. The equations presented should aid workers in this field to carry out similar analyses, as well as to check their calculations with respect to the examples described. Many of these ideas were presented at an invited lecture in Japan [35].

6 REFERENCES

1. Brot, A., "Review of Aeronautical Fatigue Investigations in Israel, April 2007 – March 2009", *Minutes of the 31st ICAF Conference,* Rotterdam, Holland, 2009.

2. Perry, J., and Perl, M., "A 3-D Model for Evaluating the Residual Stress Field Due to Swage Autofrettage," Trans. of the ASME, Journal of Pressure Vessel Technology 130, 041211 (2008).

3. Perl, M., and Bernshtein, V., "3-D Stress Intensity Factors for Arrays of Inner Radial Lunular or Crescentic Cracks in a Typical Spherical Pressure Vessel," *Engineering Fracture Mechanics*, 77, 2010.

4. Perl, M. and Perry, J., "The Beneficial Contribution of Realistic Autofrettage to the Load-Carrying Capacity of Thick-Walled Spherical Pressure Vessels," *Trans. of the ASME, Journal of Pressure Vessel Technology* 132, 011204 (2010).

5. Ma, Q., Levy, C., and Perl, M., "Stress Intensity Factors for Closely and Densely Packed Cracks in Partially Autofrettaged Pressurized Thick-Walled Cylinders," *Trans. of the ASME, Journal of Pressure Vessel Technology* 132, 051203 (2010).

6 Meyer, E. S., Rich, D. L. et al, "Fatigue Cracking in Structure Dominated by Compression Loading", Proceedings of the 23rd ICAF Conference, Hamburg, 2005.

7 Rich, D. L., Pinckert, R. E. et al, "Fatigue and Fracture Mechanics Analysis of Compression Loaded Aircraft Structure", ASTM STP 928, American Society for Testing and Materials, 1986.

8 Brot, A., " The Unexpected Behavior of Metals under Cyclic Loading Resulting from the 'Shakedown' Process ", Proceedings of the 50th Israel Annual Conference on Aerospace Sciences, 2010.

9 Freed, Y., and Rzepka, S., "An Implementation of an Accelerated Testing Methodology to Obtain Static, Creep and Fatigue Master Curves of T300/913 Unidirectional Composite Material", Proceedings of the 26th ICAF Symposium, 2011.

10 Kressel, I., Handelman, A., Botsev, Y., et al, "Health and Usage Monitoring of Unmanned Aerial Vehicles Using Fiber-Optic Sensors", Proceedings of the 26th ICAF Symposium, 2011.

11 Kressel, I., Balter, S., et al, Health and Usage Monitoring of Aging Helicopter Structure Using Fiber Bragg Grating Sensor Net", Proceedings of the 51st Israel Annual Conference on Aerospace Sciences, 2011.

12 Brot, A., "Substantiating Fatigue Lives of Structural Components Using a Weibayes Statistical Distribution ", Proceedings of the 51st Israel Annual Conference on Aerospace Sciences, 2011.

13 Yosibash Z., "Singularities in Elliptic Boundary Value Problems and Elasticity and their Connection with Failure Initiation", Springer, to be published in 2011.

14 Zaltzman T. and Yosibash Z., "Vertex singularities associated with conical points for the 3-D Laplace equation", Numerical Methods in Partial Differential Equations, to be published.

15 Yosibash Z., Shannon S., Dauge M. and Costabel M., "Circular edge singularities for the Laplace equation and the elasticity system in 3-D domains", International Journal of Fracture, to be published.

16 Buxbaum, O., Cuny, J.J., Klatschke, H. and Steinhilber, H., "Loads at the Nose Landing Gear of Civil Transport Aircraft During Towbarless Towing Operations", Proceedings of the 16th ICAF Symposium, 1991.

17 N. Konovalov, "Examination of Out-of-Plane Deformation in Three-Dimensional Crack Problems", M.Sc. Tel Aviv University, 2008.

18 Fliesher, "Examination of the Importance of Out-of-Plane Deformation for a Crack between Two Materials", B.Sc. Project, Tel Aviv University, 2008.

19 L. Banks-Sills, N. Travitzky, D. Ashkenazi and R. Eliasi, "A Methodology for Measuring Interface Fracture Toughness of Composite Materials", International Journal of Fracture, 99, (1999), 143–161.

20 L. Banks-Sills, N. Travitzky and D. Ashkenazi, "Interface Fracture Properties of a Bimaterial Ceramic Composite", Mechanics of Materials, 32, (2000), 711–722.

21 L. Banks-Sills, N. Konovalov and A. Fliesher, "The Effect of Out-of-Plane Deformation on Interface Fracture", International Congress on Fracture (ICF12), 2009a, Ottawa, Canada.

22 L. Banks-Sills, N. Konovalov and A. Fliesher,"Comparison of Two and Three-Dimensional Analyses of Interface Fracture Data Obtained from Brazilian Disk Specimens", International Journal of Structural Integrity, 1 (2010) 20–42, DOI 10.1108/17579861011023775.

23 L. Rogel, "A Through Interface Crack between a Transversely Isotropic Pair of Materials: +30°/ −60°", M.Sc., Tel Aviv University, 2009.

24 L. Rogel and L. Banks-Sills, "A Through Interface Crack between a Transversely Isotropic Pair of Materials (+30°/-60°, -30°/+60°)", Engineering Fracture Mechanics, 77 (2010) 3261–3291.

25 L. Rogel and L. Banks-Sills, "A Through Interface Crack Between a Transversely Isotropic Pair of Materials −30°/ + 60°", Composites Symposium, Technion, Israel, 2008.

26 L. Banks-Sills and L. Rogel, "Analysis of a Delamination between Two Transversely Isotropic Materials: the +30°/-60°, -30°/+60° Interfaces", European Conference on Fracture, ECF18, Dresden, Germany, 2010.

27 L. Banks-Sills and T. Ikeda, "Stress Intensity Factors for Interface Cracks between Orthotropic and Monoclinic Materials", International Journal of Fracture, 167 (2011) 47–56, DOI: 10.1007/s10704-010-9518-1.

28 Y. Motola, "Problems in Fracture Mechanics of Piezoelectric Ceramics – Analytical, Numerical and Experimental Analyses", Ph.D., Tel Aviv University, 2009.

29 Y. Motola, L. Banks-Sills and V. Fourman, "On Fracture Testing of Piezoelectric Ceramics", International Journal of Fracture, 159 (2009) 167–190, DOI 10.1007/s10704-009-9392-x.

30 L. Banks-Sills and Y. Motola, "A Fracture Criterion for Piezoelectric Material", IUTAM Symposium on Multiscale Modeling of Fatigue, Damage and Fracture in Smart Materials, Proceedings of the IUTAM Symposium on Multiscale Modeling of Fatigue, Damage and Fracture in Smart Materials, Eds. M. Kuna, A. Ricoeur, 2009, pp. 1–7, Freiberg, Germany.

31 L. Banks-Sills, Y. Motola and V. Fourman, "A Fracture Criterion for Piezoelectric Ceramics", Broberg Symposium, Eslov, Sweden, 2009b.

32 L. Heller, "A Fracture Criterion for Cracks Parallel to the Poling Direction of Piezoelectric Ceramics (PZT-5H)", M.Sc., Tel Aviv University, submitted 2011.

33 L. Heller, L. Banks-Sills, Victor Fourman and Y. Motola, "A Fracture Criterion for Cracks Parallel to the Poling Direction of Piezoelectric PZT-5H Ceramics", Israel Society for Theoretical and Applied Mechanics, Tel Aviv, Israel, 2010.

34 L. Banks-Sills, "Update — Application of the Finite Element Method to Linear Elastic Fracture Mechanics", Applied Mechanics Reviews, 63 (2010a) 020803-1–020803-17, DOI: 10.1115/1.4000798.

35 L. Banks-Sills, "Stress-Intensity Factor Calculations for Delaminations", Second International Workshops on Advances in Computational Mechanics, IWACOM-II, Yokohama, Japan, 2010.